Application of Wavelet Transform into Precise Localization of Railway Rail Edges in Visual Diagnostic of Track

Piotr Bojarczak[*]

Abstract

The paper presents the application of wavelet transform into precise localization of railway rail edges. The precise localization of inner edges of the rail is particularly crucial in detection of surface flaws by the vision system. The proposed method uses the multi-resolution analysis in detection of rail edges. Application of the wavelet transform and the choice of the right combination of decomposition levels along with wavelet type immunizes the proposed algorithm against the variation of luminance of analyzing image. The algorithm is additionally resistant to shadows incidentally appearing in analyzing images. The performance of algorithm has been tested on the images coming from real vision system installed on the carriage.

1. Introduction

At present, in Poland railway rail flaws are detected with the use of ultrasonic flaw detection device being mounted on the mobile carriage [10]. Unfortunately, such device is only able to detect flaws occurring in deeper layers of the rail. Flaws locating on the surface of rail head cannot be detected with the help of ultrasonic measurements. Needless to say that these flaws also pose a significant threat to the safety of the traffic, particularly when they are left without the supervision of their progress. There exists the method basing on eddy currents allowing for coarse determination of surface flaws, however it turns out such approach is unreliable in many cases. Tremendous progress in the development of both modern cameras and image processing algorithms allows for the creation of vision system [3], [8].

---
[*] Technical University of Radom, Malczewskiego 29, 26-600 Radom, Poland, bojarczp@wp.pl

These systems usually record the image of the rails, sleepers and the ballast with the use of fast cameras being mounted under the floor of carriage. Such system could be exploited in detection of these surface flaws. Besides the right choice of image processing algorithms locating these flaws, the precise determination of rail edges has the crucial influence on the performance of whole system. During its movement, the carriage is prone to the vibration, what in turn causes the position of rail can slightly change in subsequent frames of video stream. Therefore, it is impossible to assume the fixed position of rail in the video stream. Lin Jie et al. [12] present the method allowing for the detection of large surface flaws, however, they assume that the position of rail edges is well known. In [9], determination of rail edges is carried out with the use of Laplacian and Gaussian pyramids and morphological operations. Thanks to it, the image is decomposed into sub-images. Each next sub-image contains less detail information than its preceding sub-image. The choice of right combinations of sub-images enables to estimate approximating position of the rail. The main drawback of this method is the lack of the influence on the choice of the function using in image decomposition – only available function is the Gaussian. It deteriorates the ability of precise localization of rail edges. Babenko [1] uses to detection of rail edges traditional approach basing on Sobel filter. Additionally, Hough transform is used to settle if detected edges correspond to real four edges of rail. Such solution has two drawbacks. First, the edge detecting algorithm basing on pure gradient approach (Sobel filter) is highly dependent on luminance variation of the processing image. In order to reduce such negative effect, extra precautions should be taken, for example special shields can be mounted on the carriage. They prevent from natural light influence on the luminance of the processing image. Second, the computational complexity of Hough transform is relatively high, particularly when the resolution of processing image is high.
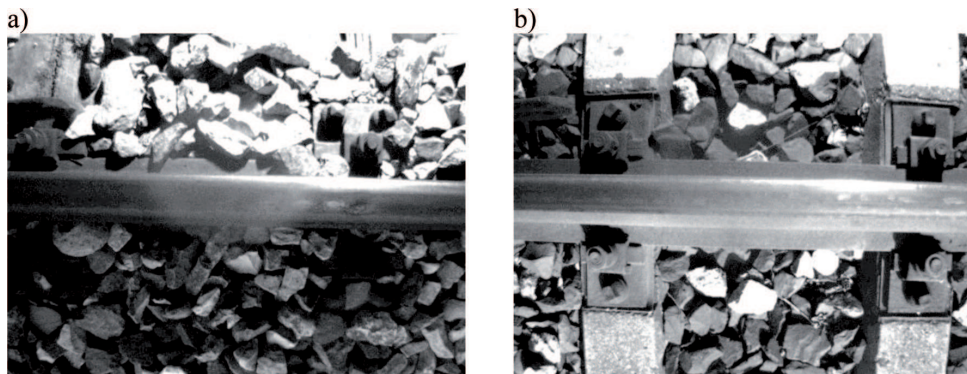

Fig. 1. a, b. Exemplary images of the track recorded by the system
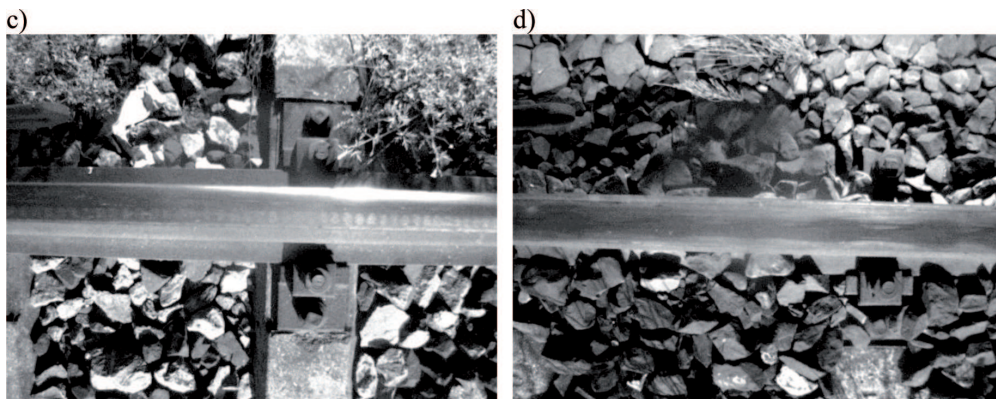
c)   d)

Fig. 1. c, d. Exemplary images of the track recorded by the system

On the other hand, the image resolution should be high, otherwise it is impossible to reliably detect surface flaws on the rail. Additionally, the image being recorded in [1] focuses mainly on the area of the rail, so that an additional camera is needed to detect other crucial objects having the influence on the safety, for example elements fastening the rail to the sleepers [4].

The author being aware of all limitations of presented methods proposed the new method basing on wavelet transform. Thanks to application of wavelet transform, it was possible to achieve high precision of rail edges detection and elimination of natural light influence on the quality of detection. The research has been conducted on images coming from the real visual system. This system was mounted as an option on ultrasonic flaw detection carriage. Its major parts constitute two fast cameras and two lamps. Lamps ensure right intensity level of recording images. It is necessary to point out that such system is not fitted with additional shields eliminating the influence of natural light on the recording images. Thanks to such solution, the compactness of the system is increased, what in turn ensures larger durability on impacts coming from incidental objects laying on the track. Another difficulty encountered during the development of rail edges detecting algorithm is the light reflection from the surface of the rail head causing the glare effect. The analysis is additionally worsened by different conditions of the railway track. Fig. 1 presents exemplary images of the resolution 1294×964 recorded by this system. All edges of the rail, depending on the condition of the track, can be fully or partially visible in the image.

All aforementioned problems cause that the development of method allowing for reliable detection of rail edges is not an easy task. Proposed solution is based on two-dimensional discrete wavelet transform (2-D DWT).

2. Wavelet Transform

Since 2-D wavelet transform is the extension of one-dimension wavelet transform, therefore its description begins from 1-D wavelet transform. 1-D wavelet transform decomposes the analyzed function on finite lasting components $\Psi(t)$ called wavelets [5], [6], [11]. Continuous-time wavelet transform (CWT) of the function f(t) generates CWT coefficients W(a,b) according to the formula:

$$W(a, b) = \int_{-\infty}^{\infty} f(t) * \Psi_{a,b}(t)dt \tag{1}$$

where:

$$\Psi_{a,b}(t) = \frac{1}{\sqrt{a}}\Psi\left(\frac{t-b}{a}\right) \tag{2}$$

is a wavelet function of time scale (dilation) equal to a and time shift (translation) described by b. For $a = 1$ and $b = 0$, $\Psi(t)$ is called the mother wavelet. If the wavelets functions are only chosen for $a = 2^k$ and $b = 2^k n$ where k and n are integer number, then formula (1) describes discrete wavelet transform (DWT) of original function $f(t)$. The wavelet transformation is reversible and the original function can be reconstructed on the basis of the values of W(a,b) coefficients. DWT can split the original function f(t) into two parts: $f_0(t)$ corresponding to coarser approximation of f(t) and $g_0(t)$ corresponding to the high frequency detail function, defined as the difference between f(t) and its approximated version. The approximated version $f_0(t)$ can be further split into two parts -coarse approximation $f_1(t)$ and the detail part $g_1(t)$. This process can be continuously performed up to some assumed level. The splitting process is often called decomposition level. For instance the first splitting process generating approximation function $f_0(t)$ corresponds to first decomposition level, the second one generating approximation function $f_1(t)$ corresponds to second decomposition level and so on. In practice the DWT is calculated with the use of two orthogonal (or biorthogonal) low-pass l(n) and high-pass h(n) filters [13]. Different wavelets correspond appropriate filter forms. The low-pass and high-pass filterings are performed step by step producing respectively, the coarse approximation of function and the coefficients containing high frequency details. In case of 2-dimensional image in each step the wavelet decomposition is performed twice: first on the rows of the image and then on its columns thus 2-dimensional (2D) DWT generates 4 sub-images for each decomposition level. Fig. 2 shows the process of generating 4 sub-images for first decomposition level.

Thanks to down sampling by 2 in x and y axes, each next decomposition level generates sub-images whose weight and height is twice smaller than weight and height of the sub-image generated in previous decomposition level. First decomposition level of Fig. 2 generates $f_{LL}(x, y), f_{LH}(x, y)$, $f_{HL}(x, y)$ and $f_{HH}(x, y)$ corresponding to smooth sub-image, horizontal details sub-image, vertical details sub-image and
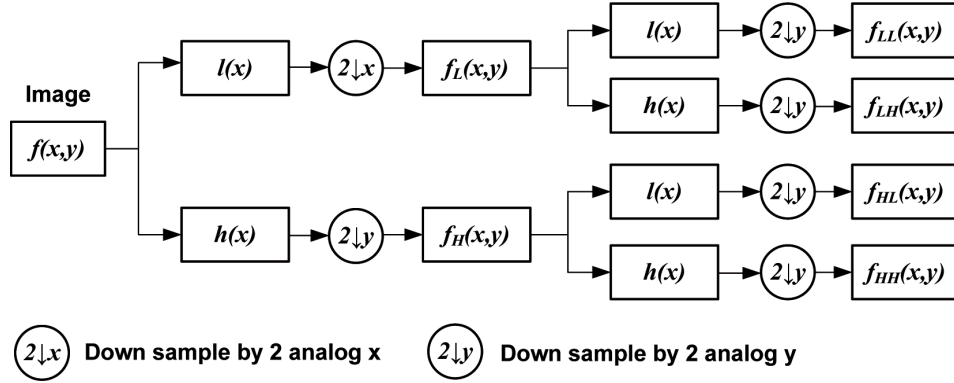
Fig. 2. Illustration of first level decomposition performed by 2D DWT

diagonal details sub-image respectively. Thanks to it, the 2-D wavelet transform is particularly useful in extraction of vertical and horizontal details of analyzing image. In addition to that, we have the influence on the size of analyzing details through the choice of proper decomposition level.

3. Description of Proposed Method

Proposed method relies on the ability of 2-D discrete wavelet transform to decomposition of the image into different levels (scales). As it was presented in Fig. 2, each decomposition level consists of four sub-images. Because the position of the rail in the image changes slightly around horizontal direction, thus the edges of rail can be determined with the help of the sub-image containing horizontal details of the original image. The most important aspect of such approach is the proper choice of wavelet type and decomposition levels. Fig. 3b and Fig. 3c present exemplary horizontal details sub-images for Bior1 and Coif1 wavelets respectively at the first decomposition level. Fig. 4 presents exemplary horizontal detail sub-images for the image of Fig. 3a for the first to fourth decomposition levels and Bior1 wavelet.

In order to choose the most appropriate wavelet type, the following wavelet families have been examined: Daubechies, Coiflets, Biorthogonal and Symlets. The sum of relative length of the upper edges obtained at the first, second, third and fourth decomposition levels has been chosen as a criterion in wavelets comparison:

$$S = \sum_{n=1}^{4} \frac{Lp_n}{Lw_n} \tag{3}$$

where: Lp_n is the part of the upper inner edge of the rail visible in the horizontal details sub-image at the n-th decomposition level, Lw_n is the full length of the upper inner edge of the rail at the n-th decomposition level.
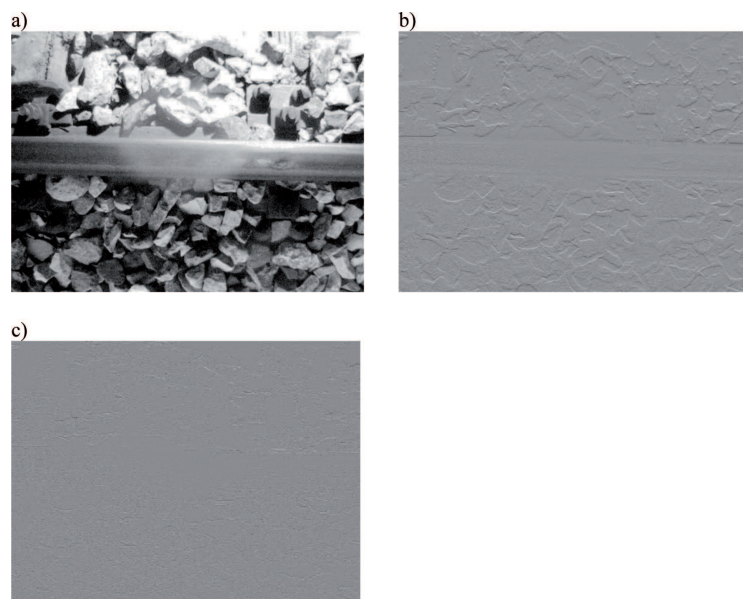
Fig. 3. Example of the choice of wavelet: a) original image b) horizontal details sub-image for bior1
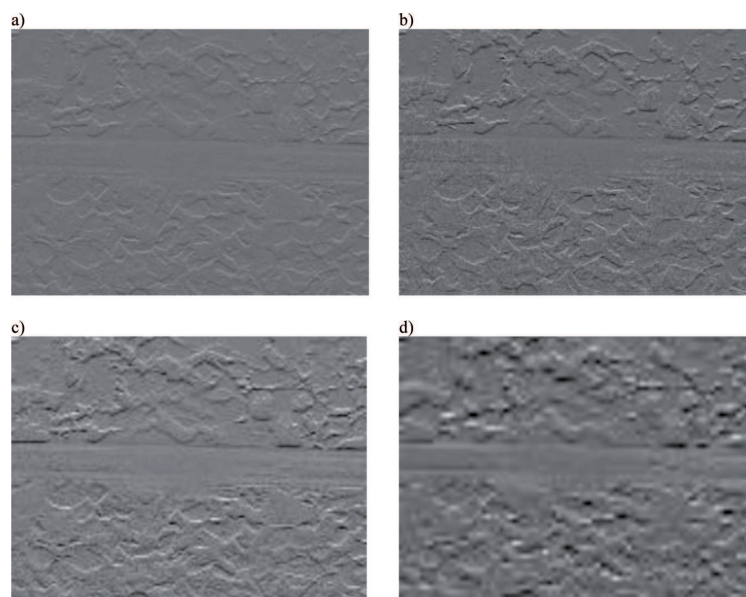wavelet, c) horizontal details sub-image for coif1 wavelet all at first decomposition level

Fig. 4. Example of the choice of decomposition level of horizontal details sub-images for the image
of Fig. 3a: a) first decomposition level, b) second decomposition level, c) third decomposition level,
d) fourth decomposition level all for Bior1 wavelet

The comparison was performed in the set of 150 images of the track randomly chosen from 1500 images. We chose the Bior1 wavelet for that average of S is maximal and variance of S is minimal.

After choosing the wavelet type we proceed with the determination of the proper decomposition level. There are at least two scenarios: Fig. 1b shows the rail with all four visible edges and Fig. 1d presents the rail with only two visible edges. In the surface flaws detecting algorithm the region of interest is only confined to the head of rail, so that we need to focus on two inner edges of the rail. Fig. 5 presents horizontal and vertical details sub-images for the image of Fig. 1b at first and third decomposition levels. Fig.6 presents also horizontal and vertical details sub-images for Fig. 1d at first and third decomposition levels. The settlement which edges occurring in horizontal details sub-image correspond to head of the rail is performed through the comparison of horizontal and corresponding vertical details sub-images. If the edge (marked as B) from horizontal details sub-image coincides with the edge (marked as A) from vertical details sub-image, then edge B from horizontal details sub-image corresponds to the edge of the head of the rail – Fig. 6. However if the edge (marked as B) from horizontal details sub-image does not coincide with the edge (marked as A) from vertical details sub-image and is placed on the right side of the edge A, then edge B also corresponds to the head of rail – Fig. 5.
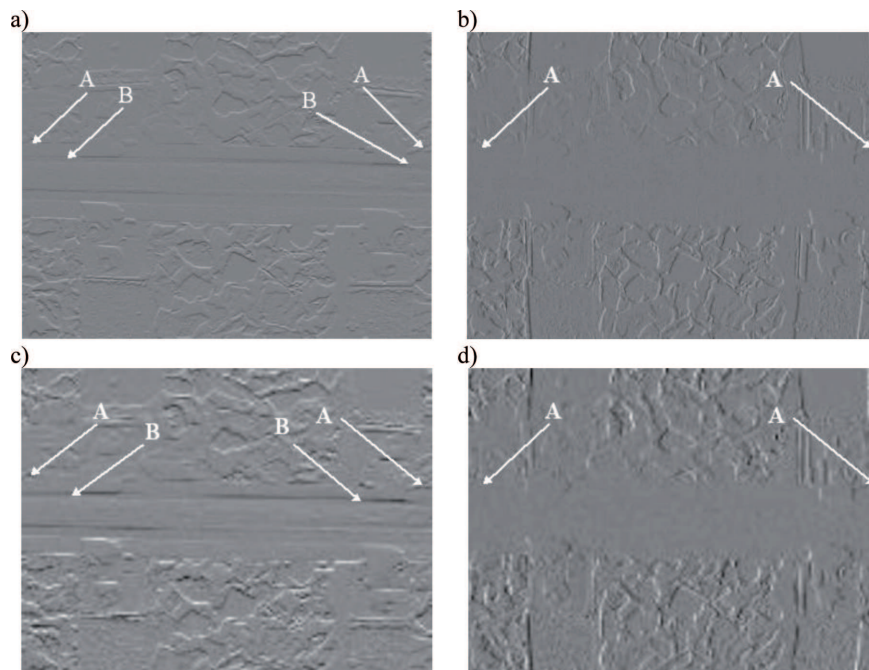

Fig. 5. Example of decomposed sub-images: a) horizontal details sub-images for image of Fig. 1b, b) vertical details sub-images all for first decomposition level, c) horizontal details sub-images d) vertical details sub-images all for third decomposition level
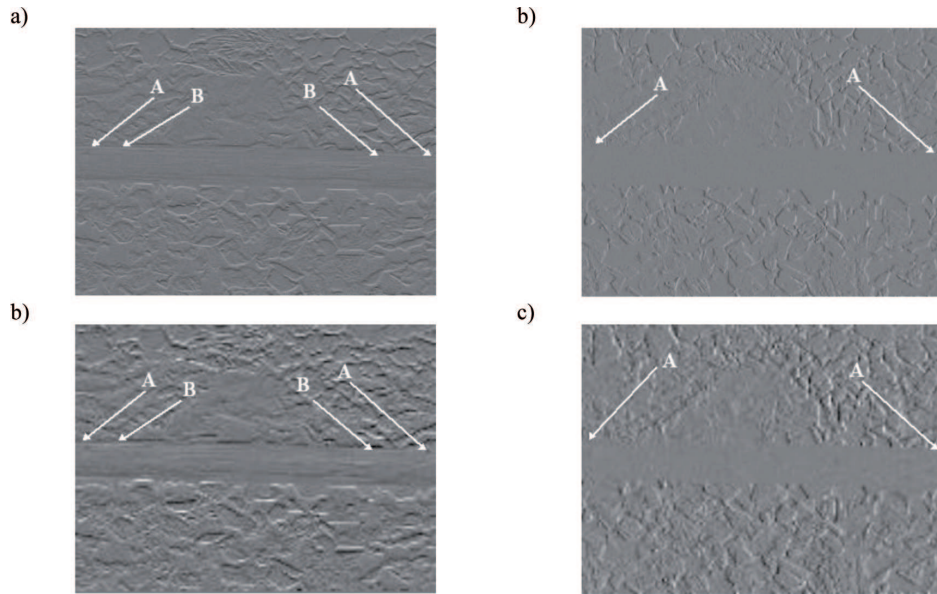
a)

b)

b)

c)

Fig. 6. Example of decomposed sub-images: a) horizontal details sub-images of Fig. 1d, b)vertical details sub-image at first decomposition level, c) horizontal details sub-image d)vertical details sub-image at third decomposition level

Because the position of the rail is biased towards horizontal direction, it is impossible to determine the edge position through simple calculation of average value of detail coefficients for each row of the sub-image and finding the row of minimal average value. In order to overcome this limitation, the whole horizontal details sub-image has been divided into eight vertical stripes. Next, for every vertical stripe the average value of details coefficients for each row has been calculated. Fig. 7 presents results of average values calculated for the first left vertical stripes of horizontal details sub-images from the Fig. 5a and Fig. 6a.
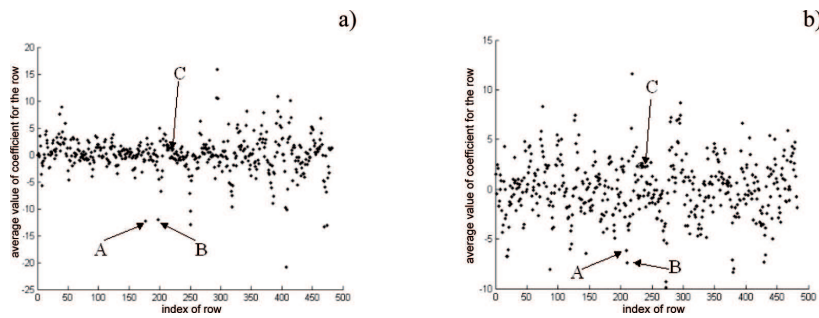
a)

b)

Fig. 7. Example of calculation of average values for the rows: a) average value of horizontal detail coefficients for rows of first left stripe of Fig. 5a, b) average value of horizontal detail coefficients for rows of first left stripe of Fig. 6a

Additionally, points corresponding to edges A and B have been marked in Fig. 7. In order to extract points corresponding to edges A and B from the Fig. 7, the position of middle horizontal line of analyzing rail (marked as C) is estimated. Vertical details sub-image corresponding to fourth decomposition level is used to estimate the position of this middle horizontal line.

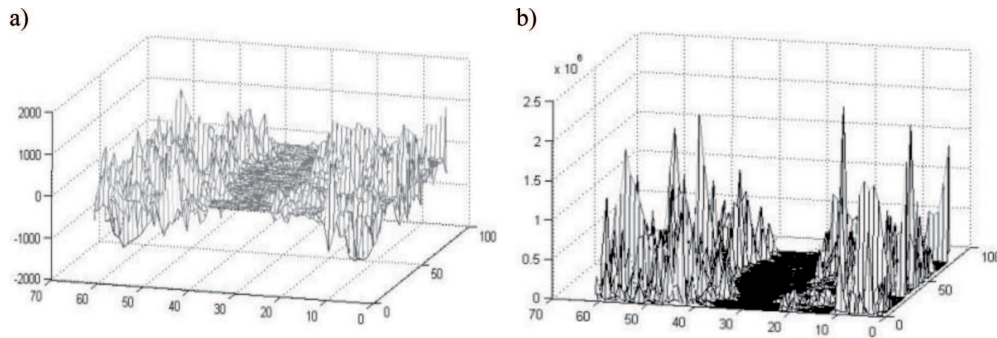a)   b)

Fig. 8. Vertical details coefficient sub-image at fourth decomposition level for the Fig. 1b: a) before, b) after enhancement

Differences between the area of the rail and the area of the ballast in the vertical details sub-image is enhanced through raising every element of vertical details sub-image to power of two. Fig. 8 presents vertical details sub-image at fourth decomposition level for the Fig.1b before and after enhancement.

The position of the middle horizontal line of the rail is estimated through the calculation of average value for each row of the vertical details sub-images from Fig. 8b. Fig. 9 presents these average values calculated for sub-images from Fig. 8. It is evident that the operation of enhancement of the sub-image allowed to obtain a significant difference between average values representing the rail and the ballast. Thanks to it, the position of the middle horizontal line of the rail is determined through simple thresholding. Threshold equal to 2100 has been chosen. Rows of average values lower than the threshold correspond to the area of the rail. Index of row marked as C corresponds to approximating position of the horizontal middle line of the rail. Because each decomposition level reduces twice the width and the height of its preceding sub-image, it is readily to determine the row index in horizontal details sub-image for first decomposition level on the basis of the row index of vertical details sub-image for fourth decomposition level – Fig. 9b. It is calculated according to the formula:

$$I\_row1 = 8^*I\_row4 \qquad (4)$$

where: I_row1 is the row index for the sub-image of first decomposition level and I_row4 is the row index for the sub-image of fourth decomposition level.

Once the index of row corresponding to middle horizontal line of rail is determined, the position of rail edges A and B in Fig. 7 can be easy found by searching

two lowest values in the window of the length of 40 located on the left side of point C. The last element of this window is the point C. The length of this window has been chosen at the assumption that the angle of bias of the rail varies from 0^0 to 8^0. The placement of the cameras on the four-wheel truck instead of the carriage floor caused that the bias of the rail towards horizontal direction is confined to small angle, even when the carriage moves on the arc of the track.
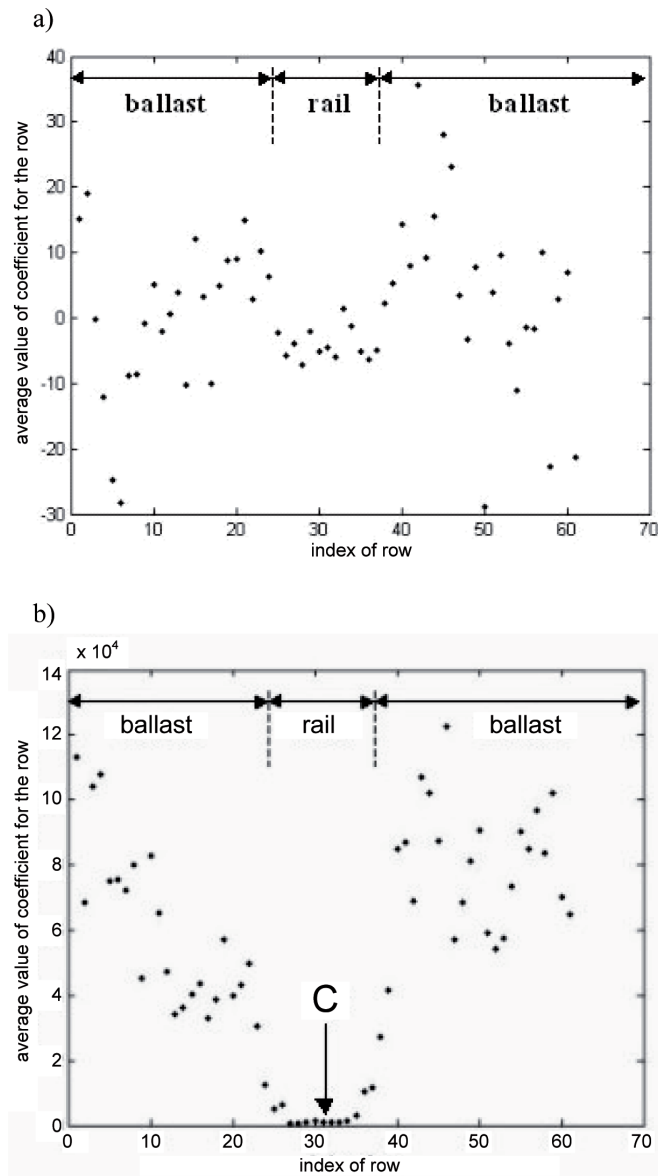
a)

b)

Fig. 9. Average values for rows of the vertical details sub-images a) from Fig. 8a, b) from Fig. 8b

Presented algorithm is repeated for each of vertical stripe of the horizontal details sub-image of first decomposition level. Thanks to it, it is possible to estimate the average position of rail edges A and B for each vertical stripe. The choice of the number of vertical stripes is a tradeoff between the precision in localization of rail edges and the resistance of the algorithm to the noise occurring in the horizontal details sub-image. An increase of the width of the vertical stripe reduces the precision of localization of the rail edges and enhances the resistance to the noise. After conducting the experiment we decided to choose eight vertical stripes, so that the algorithm generates eight average positions of rail edges, each of them corresponding to the part of the image represented by the corresponding vertical stripe. Final localization of the rail edge is carried out with the use of robust linear squares fitting algorithm [2], [7]. Fig. 10 presents effect of rail edges localization for images from Fig. 1b and Fig. 1d. Because fixed distance between the camera and the surface of the track is kept, the algorithm needs only to detect the upper inner edge of the rail, the bottom inner edge is drawn on the basis of the upper edge. Additionally, the average localization of edge for each vertical stripe marked with white rectangle has also been presented.
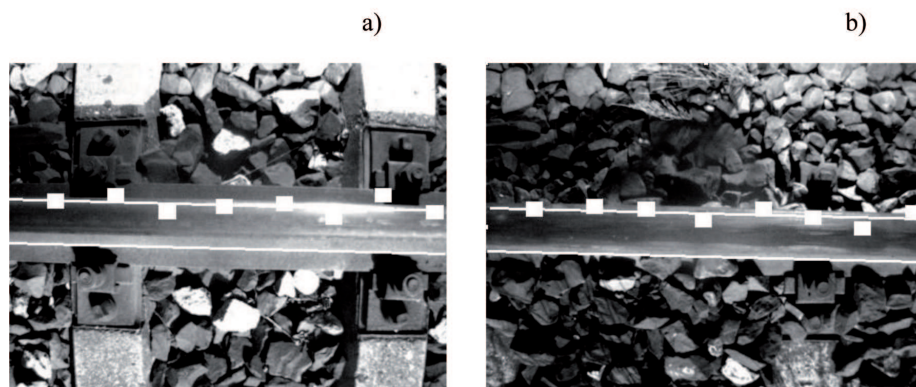
a)   b)

Fig. 10. Results of rail edges detection for images from: a) Fig. 1b, b) Fig. 1d

4. Conclusion

The algorithm has advantages towards solutions presented in [1], [9]. The main advantage is the resistance to the change of luminance of analyzing image. Detection of rail edges is realized with the use of wavelet transform, that decomposes analyzing image into the sets of horizontal and vertical details sub-images. Thanks to such approach, the algorithm is additionally resistant to shadows incidentally appearing in the image. Presented solution does not require installation of extra shields preventing from the change of luminance of the image. The precise localization of the inner

edges of the rail is a crucial in detection of surface flaws of the rail. The right performance of algorithm was checked in the set of 500 images randomly chosen form the huge data base of images recorded by visual system. In next stage, we are going to develop the algorithm allowing for detection of these types of flaws.

References

1. Babenko P.: Visual inspection of railroad tracks, Doctoral Thesis, University of Central Florida, Orlando, 2009.
2. Bevington P. R., Robinson D. K.: Data Reduction and Error Analysis for the Physical Sciences, 2nd Ed., WCB/McGraw-Hill, Boston, 1992.
3. Bojarczak P., Lesiak P.: Zastosowanie hybrydowej sieci neuronowej do klasyfikacji drewnianych podkładów kolejowych, Prace Naukowe, Transport, Politechnika Warszawska z.78, 2011.
4. Bojarczak P., Lesiak P.: Visual system diagnosing the state of elements fastening the rail to the sleepers, Pomiary, Automatyka, Kontrola, 12/ 2011.
5. Bovik A.: Handbook of Image and Video Processing, Academic Press, 2000.
6. Daubechies I.: Ten lectures on wavelets, SIAM Press, 1988.
7. Draper N. R., Smith H.: Applied Regression Analysis, 3rd Ed., John Wiley & Sons, New York, 1998.
8. Kędra Z.: Diagnostyka obrazowa rozjazdów kolejowych, Logistyka 6/2011(CD).
9. Khandogin I., Kummert A., Maiwald D.: Nonlinear image processing for automatic inspection of railroad lines, IEEE Workshop on Nonlinear Signal and Image Processing, Michigan, USA, 1997.
10. Lesiak P.: Diagnostic technology of contact-stress flaws such as head checking in railway rails, Monograph No 121,Technical University of Radom, 2008.
11. Lesiak P., Bojarczak P.: Application of Wavelets and Fuzzy sets to detection of head checking defects in railway rail, Transport Systems Telematics , 10th Conference TST 2010, Communications in Computer and Information Science 104, Springer 2010.
12. Lin Jie, Luo Siwei, Li Qingyong, Zhang Hanqing, Ren Shengwei.: Real-time Rail head surface defect detection: a geometrical approach, IEEE International Symposium on Industrial Electronics, Seoul, Korea, 2009.
13. Mallat S.: A theory for multiresolution signal decomposition: the wavelet representation, IEEE Trans. PAMI, vol 11, 1989.